ELSEVIER

Improved BOLD detection in the medial temporal region using parallel imaging and voxel volume reduction

Patrick S.F. Bellgowan,[a],* Peter A. Bandettini,[b,c] Peter van Gelderen,[d]
Alex Martin,[a] and Jerzy Bodurka[b]

[a]*Section on Cognitive Neuropsychology, NIMH, 10 Center Drive, 10 Center Dr., Bldg 10 room 4C104, NIH, Bethesda, MD 20892-1366, USA*
[b]*Functional MRI Facility, NIMH, 10 Center Drive, Bethesda, MD 20892, USA*
[c]*Section on Functional Imaging Methods, NIMH Center Drive, Bethesda, MD 20892, USA*
[d]*Advanced MRI Section, NINDS, 10 Center Drive, Bethesda, MD 20892, USA*

Using gradient-echo EPI, signal dropout due to macroscopic off resonance effects can prevent blood-oxygenation-level-dependent (BOLD) signal change detection. The anterior medial temporal lobe (MTL) is located near these susceptibility gradients and therefore shows considerable signal dropout with GE-EPI. Reducing the volume of the image voxel reduces susceptibility-related signal dropout. However, this is accompanied by a prohibitive reduction in signal-to-noise ratio (SNR). To compensate for SNR loss with smaller voxels, we used a multi-channel MRI receiver with an array of receive-only 16-element surface coils at 3 T. We demonstrate that the reduction of susceptibility artifacts, through use of high resolution images, coupled with the gains in image SNR from the array coil improves the temporal signal-to-noise ratio (TSNR) and enhances the contrast-to-noise ratio (CNR). Furthermore, a comparison of 2 mm with 4-mm-thick axial images both with the same in-plane resolution showed that thinner slices enhanced TSNR and CNR throughout the ventral – medial regions of the temporal lobes, with the greatest improvement in the most anterior regions of the MTL. Further improvements were seen when adjacent 2 mm slices were combined to match overall voxel volume. These results demonstrate that BOLD investigation of anterior MTL function can be enhanced by decreasing voxel size but only in combination with the SNR gained by using the 16-channel head coil system.
Published by Elsevier Inc.

Keywords: MRI imaging; BOLD; Susceptibility; MTL

Introduction

Understanding the functional role of the medial temporal lobes in neurologically normal subjects (Brewer et al., 1998; Squire et al., 2004; O'Kane et al., 2005; Strange et al., 2005) and patient groups (Bellgowan et al., 1998; Golby et al., 2002, 2005; Janszky et al., 2005) has been greatly enhanced by functional magnetic resonance imaging (fMRI) techniques. However, initial attempts to use fMRI to study the medial temporal lobes, including the hippocampus, were inconsistent. Two methodological factors may account for this inconsistency. First, early declarative memory studies failed to recognize the significance of a proper baseline condition (Martin et al., 1997; Binder et al., 1999; Stark and Squire, 2001). Thus, contrasts were made between tasks that each activated the hippocampus to some extent, including the baseline condition. Second, the MTL is located in a region of large susceptibility variations. The medial temporal lobes are partially surrounded by bone and tissue interfaces including air-filled spaces like the nasal sinuses, ear cavities, and perforated bone. Magnetic susceptibility differences at air tissue or bone/tissue interfaces create magnetic field gradients resulting in severe intra-voxel phase dispersion, which in turn, results in image distortions in gradient-echo and spin-echo echo planar imaging (EPI)—proportional to the readout window duration and signal dropout in gradient echo-planar EPI (Fischer and Ladebeck, 1998; Schmidt et al., 2005a). Several approaches have been proposed to compensate for this static field effect, including asymmetric spin-echo (Stables et al., 1998; Schmidt et al., 2005a), and the use of tailored radiofrequency pulses (Cho and Ro, 1992). Sampling k-space in a spiral pattern has also been suggested as an approach to reduce signal dropout (Glover and Law, 2001). Compared with an echo-planar imaging scheme, spiral acquisition offers the option to use a shorter TE with single shot acquisition and less geometrical distortion with off resonance effects. However, the corresponding shorter echo time may not be optimal for maximal BOLD contrast (Menon et al., 1993) in other regions with longer T2*. Another approach to compensate for unwanted effects from local background gradients has been to use Z-shimming (Glover, 1999). In this method, multiple images with

---

* Corresponding author. Fax: +1 301 402 0921.
E-mail address: psfb@mail.nih.gov (P.S.F. Bellgowan).
Available online on ScienceDirect (www.sciencedirect.com).

different slice refocusing gradients are collected and combined. However, original Z-shimming methods required a doubling in acquisition time. More recent Z-shimming developments utilize half k-space acquisition. This modification improves temporal resolution (Stenger et al., 2002; Guo and Song, 2003) and has been shown to reduce dropout in both the orbital–frontal gyrus and portions of the MTL. However, this procedure requires additional post-acquisition processing and does not improve SNR. SENSE imaging has recently proven to be useful in reducing susceptibility artifacts in the MTL when moderate SENSE levels are used (Schmidt et al., 2005a). However, like the half k-space technique, SENSE imaging alone does not provide enough SNR to image at high resolution. The use of para-magnetic oral passive shims is another technique that has been effective in reducing susceptibility artifact (Wilson et al., 2003). However, passive shimming requires creating and calibrating an intra-oral shim. As a result, this technique may be less useful for studies that seek to evaluate BOLD changes over multiple sessions. Recently, Wong and Mazaheri (2004) proposed using an external local shim coil to compensate for the field inhomogeneities, and Hsu and Glover (2005) proposed using a resistive shim coils placed in the mouth. Like passive oral shims, these methods would require prior tuning and a series of placement scans to optimize shim coil performance.

A straightforward solution to correct for susceptibility-related signal dropout would be to reduce intra-voxel dephasing and intra-voxel tissue heterogeneity (CSF, gray matter (GM), and white matter (WM)) by reducing voxel size, especially in the slice (in-plane (z)) direction (Merboldt et al., 2000; Wadghiri et al., 2001). However, because signal is proportional to voxel volume, decreasing slice thickness reduces signal-to-noise ratio (SNR). Merboldt et al. (2000) showed that decreasing slice thickness improves signal dropout in inferior regions of the brain, but it also decreases BOLD contrast-to-noise ratio (CNR). This CNR decrease was attributed to a SNR reduction due to increased spatial resolution. One solution to this problem is to acquire alternating thin slices on consecutive TRs and add adjacent slices to recover lost SNR (Merboldt et al., 2000). Though this approach reduces signal dropout and may recover SNR, the gains in spatial and temporal resolutions are limited.

Recent advances in MRI receiver and coil technologies have led to the development of multi-element receive-only surface coil arrays, suitable for the whole brain imaging, that greatly enhance SNR (Bodurka et al., 2004; de Zwart et al., 2004). Close proximity to the head and multiple measures within the FOV provide arrayed surface coils with a distinct advantage in SNR as compared to standard transmit/receive birdcage coils. The 16-element array coil used in this report offers an overall 3-fold SNR improvement as compared to standard birdcage head coil during EPI acquisition (de Zwart et al., 2004). The current study also takes advantage of the increased SNR available with a highly sensitive MR receiver/detector system for EPI fMRI at 3 T. The gain in SNR allows for higher spatial resolution fMRI. We also evaluated the effect of increasing fMRI spatial resolution by reducing slice thickness to determine if this would help to recover signal susceptibility-related MR signal dropout in anterior MTL regions. We predicted that, at higher EPI resolution (thinner slices), the gain in image SNR would translate to improved EPI image-to-image stability (TSNR) and enhanced BOLD signal detection (CNR). However, the cost of reducing voxel volume is a reduction in the imaging volume coverage per unit time.

Materials and methods

Participants

Twelve right-handed, fluent English-speaking adults (ages 22–34) participated for approximately 2 h in experiments 1 ($N = 4$, two female) or 2 ($N = 8$, five female). All subjects signed informed consents in compliance with the IRB at NIH and were monetarily compensated for their participation.

Imaging

All subjects were scanned on a 3 T General Electric (GE) Signa VH/3 MRI scanner (3 T/90 cm, gradient strength 40 mT/m, slew rate 150 T/m/s, whole body detunable transmit/receive (T/R) RF coil)) equipped with a home-built scalable multi-channel MRI digital receiver (Bodurka et al., 2004). Two systems were used for MRI signal reception. The first was a standard system equipped with a birdcage transmit/receive RF coil connected to a standard GE receiver. The second system utilized an array coil consisting of 16 receive-only surface coils (de Zwart et al., 2004) attached to a home-built sixteen channel MRI receiver (Bodurka et al., 2004). For all subjects, 16 axial slices were collected using a single-shot, full k-space gradient-echo echo-planar (EPI) sequence (TR = 2000 ms, TE = 40 ms, flip angle = 90°, FOV = 200 mm, and in-plane resolution 3.125×3.125 mm^2, slice thickness = 2 mm or 4 mm, number of volumes = 132, EPI readout duration = 35 ms). For the standard birdcage RF coil, EPI acquisition data were collected using a single-channel GE fast receiver (250 kHz sampling bandwidth). For the array coil, EPI data acquisition was done in parallel with the home-built 16-channel MRI receiver (sampling bandwidth 500 kHz per channel). Individual EPI array coil magnitude images were reconstructed from raw data and combined (square root of sum of individual square magnitude images) into a final image. High resolution anatomical whole brain images were acquired using a magnetization-prepared rapid acquisition gradient-echo imaging sequence (MPRAGE) (FOV = 220 mm, slice thickness = 1.2 mm, and in-plane resolution = 1.0×1.0 mm^2).

Two functional experiments were conducted. In the first experiment, we compared TSNR using the 16-element coil and the standard birdcage GE head coil. The order of which head coil was used was counterbalanced across subjects. TSNR was calculated on a voxel-wise basis as the ratio of the average image magnitude over the time course standard deviation using AFNI after within run image registration (Cox, 1996; Cox and Hyde, 1997; Cox and Jesmanowicz, 1999). Both the average and standard deviation values were calculated using the entire time with the first four volumes removed to allow for steady-state equilibrium. We chose to compare TSNR rather than SNR because signal extraction in fMRI experiments is dependent on a temporal component. TSNR reflects EPI image-to-image temporal signal stability and therefore is a more direct measure of fMRI sensitivity than individual image SNR.

In the second experiment, only the 16-channel coil was used. In this study, we measured TSNR and CNR (the full model F statistic from a multiple linear regression analysis) at 2 and 4 mm slice thickness, as well as with 4 mm slices created by combining adjacent 2 mm slices ("2 + 2" mm condition). In both studies, the scanning parameters and slice locations were limited to the temporal and occipital lobes and ventral orbital frontal cortex.

The most inferior slice location was matched between the acquisition of the 2 mm and 4 mm acquisitions.

Tasks and stimuli

Participants performed alternating spatial and object memory tasks known to require participation of the MTL (Buffalo et al., 1998). Both tasks involved a 30 s encoding period, followed by a 30-s delay period, followed by a 30-s recognition memory test period. This sequence terminated with a 30-s delay period prior to the onset of the next encode–delay–recognition memory cycle. Two of these cycles were repeated for both the spatial and object memory tasks during each functional scan. Stimulus presentation parameters were equivalent during both memory tasks. During encoding, subjects were presented with a sequence of six fractal images to learn. Subjects were instructed to respond by button press to acknowledge the presentation of each fractal. Fractals were presented for 500 ms in any of 12 locations distributed throughout the screen. The post-encoding delay consisted of six presentations of a scrambled image located in the center of the screen with instructions to respond by button press to acknowledge stimulus presentation. Recognition memory blocks consisted of another sequence of six fractals, including three fractals that had been previously presented during the encoding/learning period (target stimuli). Subjects responded by button press to indicate a previously presented fractal. The order of the memory task type (object or spatial memory) and slice thickness acquisition were counterbalanced across subjects.

Results

Behavioral data

D-prime scores indicate that subjects were able to successfully perform both the object and spatial memory task. Consistent with Buffalo et al. (submitted for publication), recognition memory performance did not differ between tasks ($F < 1.0$).

Imaging data

Fig. 1 depicts the average TSNR difference maps between the standard system and 16-element array head coils. The TSNR across all four runs was averaged on a voxel-wise basis for each subject. Results showed greater TSNR (>50%) across all voxels (Fig. 1) acquired with the parallel MRI receiver equipped with the 16-element array coil. This difference replicates previous findings showing a significant SNR advantage when using the 16-channel coil configuration (de Zwart et al., 2004).

One of the more significant benefits to neuroscientist using this MRI coil design is to achieve a higher spatial resolution (Beauchamp et al., 2004). Serendipitously, higher spatial resolution should be accompanied by less partial volume effects and reduction of susceptibility-related signal dropout. Thus, the next experiment investigated the effect of reducing slice thickness on signal dropout and partial volume effects using the 2 mm, 2 + 2 mm, and 4 mm slice thicknesses with the 16-element array coil. Fig. 2 shows representative SNR (upper row) and TSNR (lower row) maps collected from an individual subject for each slice thickness. Thicker slices (4 mm) clearly show greater SNR than thinner (2 mm) slices, however, this difference is reversed when voxel volume is equated (2 + 2 mm). The improvement in SNR by adding adjacent thin slices compared to a single thinner slice is likely due to the reduction in signal dropout that occurs when thinner slices are used. The bottom row of Fig. 2 clearly shows greater TSNR in medial anterior temporal regions for the thinner slices (2 mm). This difference was increased when voxel volume was equated at 4 mm. Although it is counterintuitive to see greater TSNR in areas with less SNR, this effect may result from a non-linear relationship between the two measures of signal strength (Kruger and Glover, 2001). Thinner (2 mm) slices showed less signal dropout than thicker 4 mm slices in medial temporal regions.
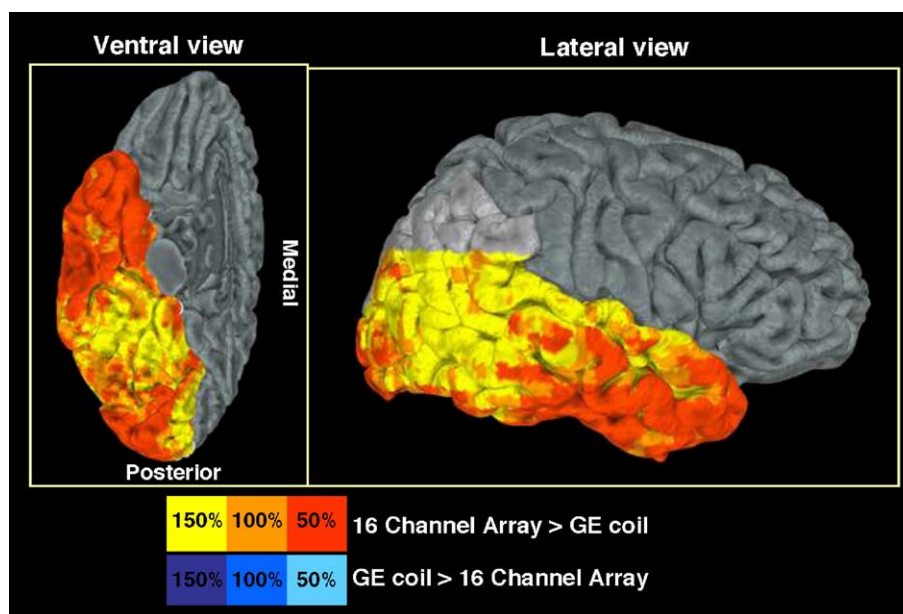

Fig. 1. TSNR comparison in the same subjects scanned using the 16-channel coil relative to standard GE quadrature head coil. These images are rendered surface volumes of the lateral and medial surfaces of the left hemisphere. These differences were similar across hemispheres.
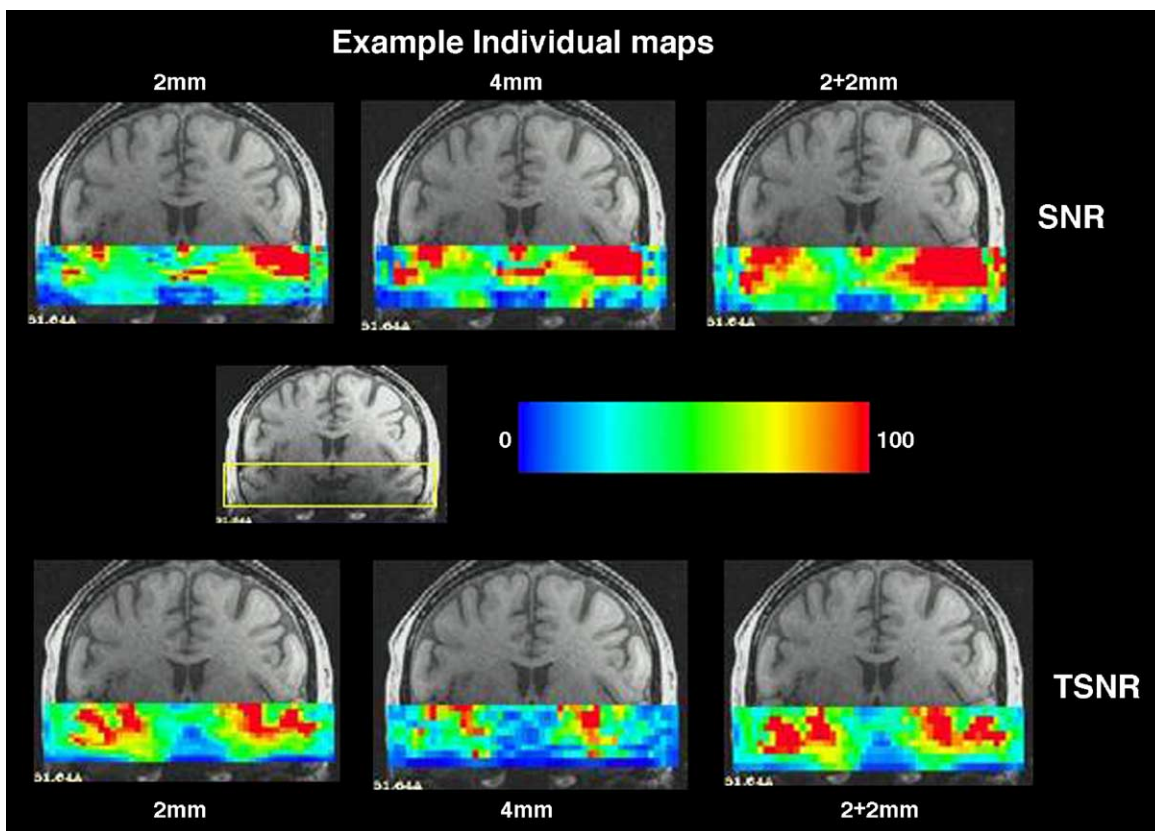
Fig. 2. Representative SNR and TSNR maps for an individual subject are shown. The top row depicts the SNR values overlaid on the high resolution anatomical images for the 2 mm, 4 mm, and 2 + 2 mm conditions. The bottom row depicts the TSNR measures for the same subject at the same slice locations as the above SNR measures. Again, the columns depict the 2 mm, 4 mm, and 2 + 2 mm conditions respectively. The middle row depicts the imaged region for the 2 mm condition and the color scale used for depicting both the SNR and TSNR maps.

Although this recovered signal is not enough to equate the thin and thick slices using a SNR measure, the recovered signal in the thinner slices contributes positively to the signal component of the TSNR measure, thereby enhancing the TSNR for the 2 mm but not 4 mm thick slices.

To quantify these differences, subjects' mean TSNR maps for the three slice thicknesses (2 mm, 4 mm, and 2 + 2 mm) were submitted to a voxel-wise mixed-effects ANOVA with subjects as a random factor and slice thickness as a fixed factor. Mean TSNR maps were created by averaging each of the four runs for the 3 slice conditions. Individual mean TSNR maps were then spatially normalized without application of a blurring filter (beyond the "nearest neighbor" smoothing involved in stereotaxic normalization). A priori t test comparison of means results were masked so that they contained only the volume imaged using 2 mm slice thickness. t test results, depicted in Fig. 3, show significantly greater TSNR for 2 mm slices in select regions of the orbital frontal gyrus, anterior temporal pole, anterior parahippocampal gyrus, middle temporal gyrus, entorhinal cortex, and lateral inferior and middle temporal gyri, amygdala, posterior hippocampus, and anterior fusiform. These differences were potentiated when "2 + 2" mm slices were compared to 4 mm slices such that significant activation extended more posteriorly along the parahippocampus and fusiform gyrus to the occipital pole. Regions showing significantly greater TSNR with 4 mm slices include inferior frontal regions, cerebellum, posterior medial fusiform gyrus, and lateral middle temporal gyrus. Consistent with our hypothesis, the results depicted in Fig. 3 suggest that increases in measured TSNR for 2 mm relative to 4 mm slice thickness are dominant in areas vulnerable to MR signal dropout. However, the contribution of task-related variance may bias the measured TSNR differences because the TSNR measure reflects fMRI signal variability. Task-related variance, particularly in block designs, produces large systematic changes in MR signal intensity. These large fluctuations may overshadow smaller TSNR improvements related to a reduced influence of the noise components. Therefore, we investigated BOLD CNR as an additional measure of estimating improvements related to slice thickness reduction. Because CNR takes into account task-related variability, it should be more sensitive to the influence of other sources of noise (e.g. vessels, WM, and CSF contributions).

As a measure of CNR, we used the full-model F statistic, calculated from the imposed memory tasks relative to a passive baseline condition (pre-encoding) for each subject. The F statistic was used as the measure of CNR because it can estimate the task-related variability for all three conditions simultaneously. The F statistic was calculated for each concatenation of runs for each of the different slice thickness. Concatenated runs for either the 2, 4, or "2 + 2" mm conditions were submitted to multiple regression analysis using three regressors corresponding to the encoding, post-encoding delay, and recognition cycles. The full-model F statistic for all slice thickness conditions was put into standardized space as described above and submitted to a voxel-wise ANOVA (see Fig. 4).
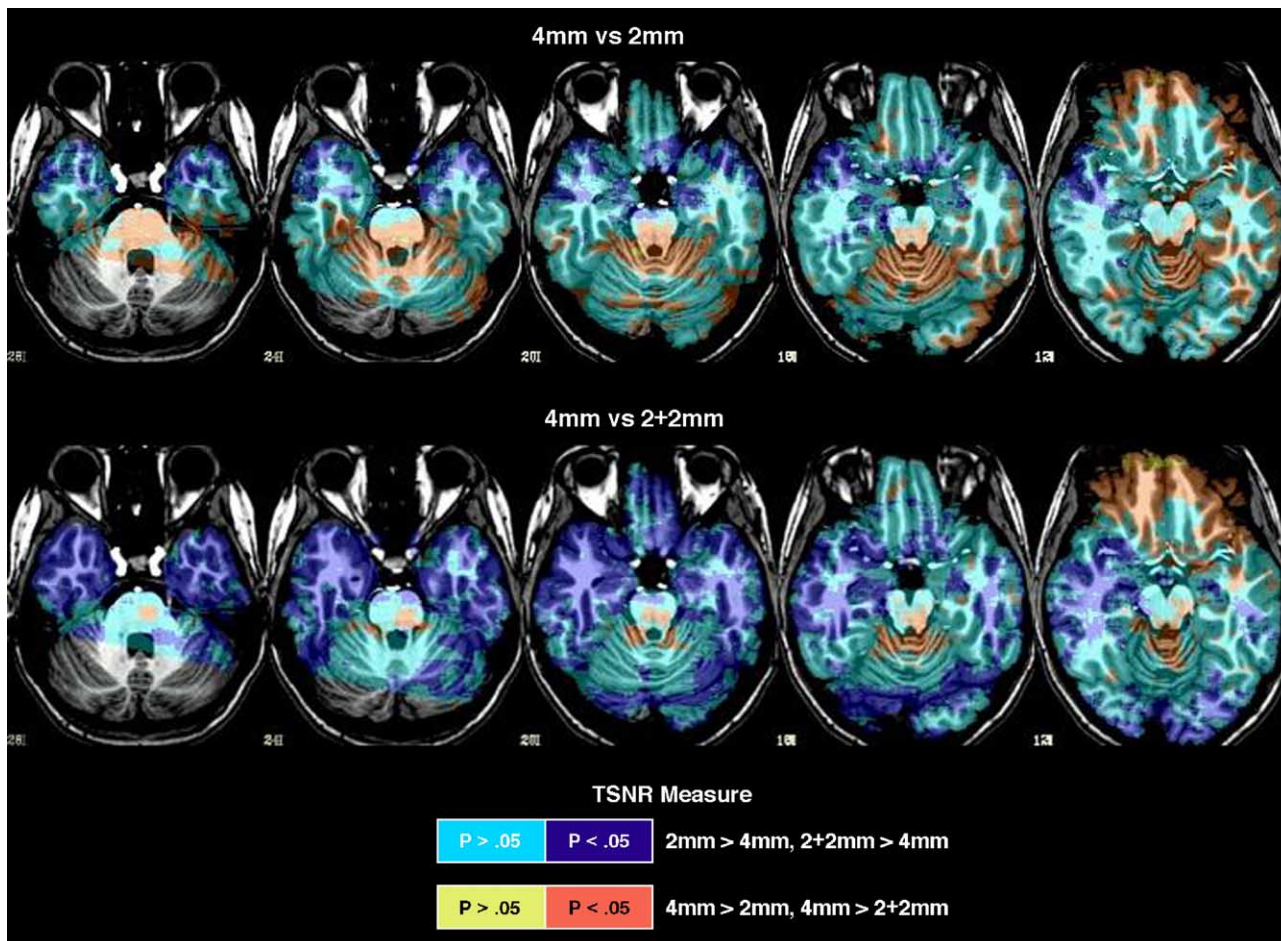
Fig. 3. A priori contrast of means maps are depicted showing both the statistically significant voxels (orange and purple) and the direction of the non-significant voxels when comparing TSNR between 2 mm and 4 mm (upper row) and 2 + 2-mm and 4-mm (lower row)-thick slices using the 16-channel arrayed coil. Cool colors represent areas showing greater TSNR for 2 mm and 2 + 2 mm thick slices, and warm colors represent the converse.

Thinner slices improved CNR in much of the anterior and medial temporal regions, posterior orbital frontal gyrus, para-hippocampus, fusiform, and occipital cortex. Importantly, CNR showed improved signal detection for thinner slices in regions important for memory function including the perirhinal, entorhinal, and inferior temporal cortex. Unlike TSNR, CNR accounts for task-related changes and therefore showed the greatest improvements in BOLD contrast in regions active during task performance.

Discussion

Understanding the functional properties of the anterior MTL and ventromedial prefrontal cortex using fMRI has been hindered by this regions' sensitivity to susceptibility artifacts. The present experiments showed significant improvements in both TSNR and CNR for most of the imaged volume, particularly those regions sensitive to susceptibility artifacts. These imaging improvements were obtained by using advanced head coil and receiver technology providing substantial SNR improvements that allowed us to decrease the in-plane slice thickness. Although slice thickness reduction can result in insufficient SNR to detect small BOLD responses, the current experiment offsets this deficiency by using a 16-channel array coil and MRI receiver system. Specifically, the

results from Experiment 1 demonstrate a significant increase in TSNR using parallel imaging with the 16-channel array coil relative to single-channel data acquisition with the standard birdcage GE head coil. The second study showed that the advantage gained using the 16-channel coil/receiver system can be used to increase spatial resolution. Higher spatial resolution led to significant improvement in TSNR and particularly in CNR throughout most temporal and occipital regions, including the anterior medial temporal lobe and ventromedial prefrontal cortex.

Several models of BOLD signal formation suggest that improvements in both SNR and BOLD CNR can be obtained with higher field strengths (Menon et al., 1993, Hyde et al., 2001). However, the physiological noise present in gradient recalled EPI fMRI data also correlates positively with MRI signal strength (Kruger and Glover, 2001). To further elucidate the relationship between MR field strength and obtainable signal, Kruger and Glover (2001) proposed a model of the relationship among TE-dependent and non-TE-dependent physiological noise and SNR. In this physiological noise model, "achievable" TSNR is distributed in an asymptotic function relative to TE-dependent noise, suggesting that the level of measured SNR has a rate-limiting effect on the contribution of noise to the EPI signal. Kruger and Glover (2001) demonstrated support for their model by experimentally showing that increases in SNR at 3 T caused TSNR
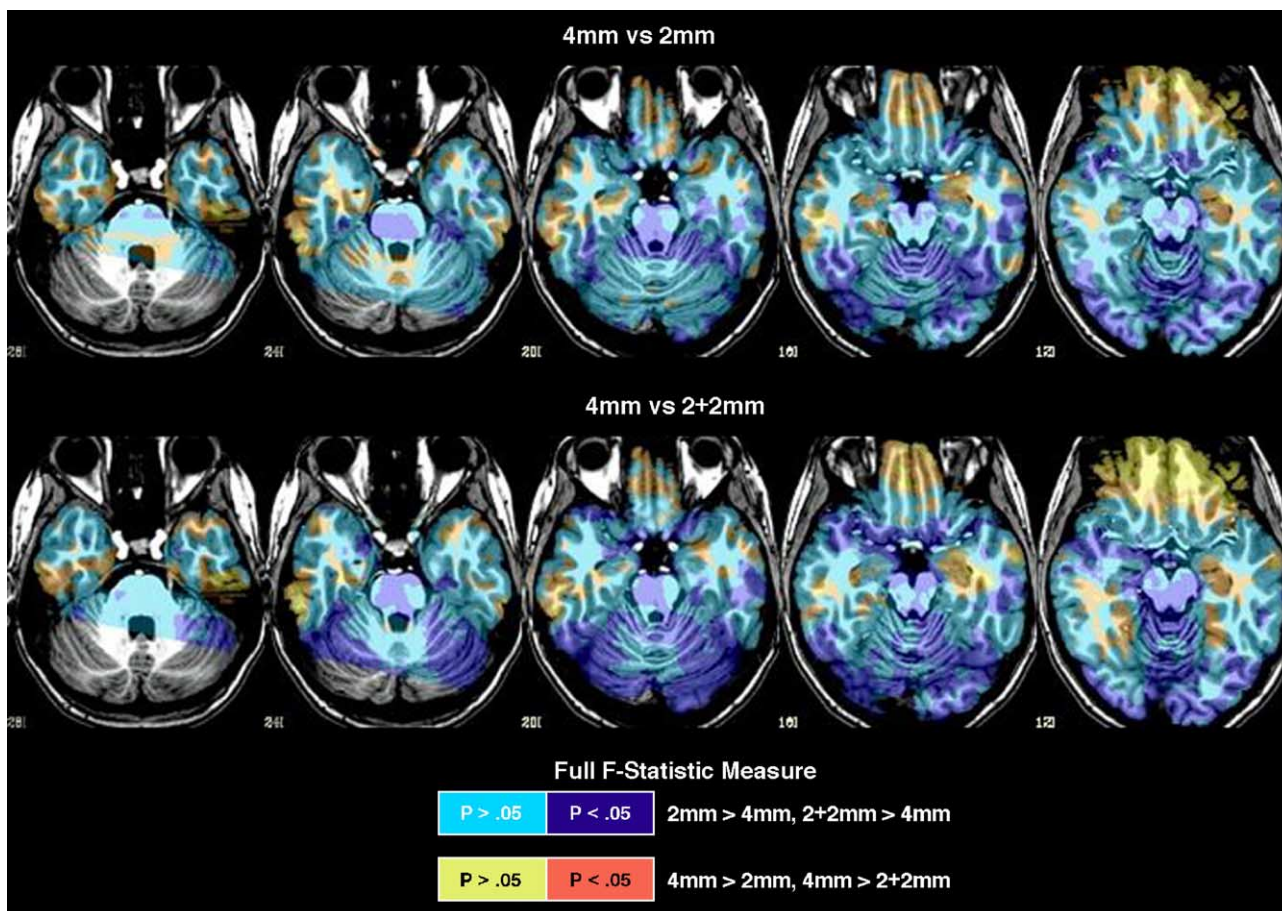
Fig. 4. These maps show both the statistically significant and the direction of the non-significant voxels for a priori contrast of means comparing differences in CNR between the 2-mm and 4-mm (upper row) and 2 + 2-mm and 4-mm (lower row)-thick slices. All data were collected using the 16-channel arrayed coil. CNR was defined using the full model F statistic in individual multiple regression analyses. Cool colors represent areas showing greater CNR for 2-mm and 2 + 2-mm-thick slices, and warm colors greater activation for 4 mm slices.

saturation in BOLD imaging. Recently, this prediction has also been confirmed at 7 T (Triantafyllou et al., 2005). The implication of this effect is that, in areas with high SNR, such as those in posterior occipital and occipito-temporal cortices, small changes in noise properties will have a limited effect on BOLD detection. However, areas with less SNR may be more sensitive to small changes in noise levels such as those produced by slice thickness reduction.

Results of our experiments demonstrated a significant increase in TSNR using the 16-element array coil relative to standard birdcage GE head coil. The increase in SNR allows for the use of higher fMRI spatial resolution (2 mm slices). Thinner slices were used to test whether sufficient SNR exist in specific structures of the MTL to enhance BOLD detection. Compared to standard resolution fMRI (4 mm slices), high resolution fMRI yielded significant improvement in BOLD CNR in the anterior medial temporal lobe. This suggests that, when using smaller voxel sizes (voxel volume $\sim$ 30 mm^3), at 3 T with the 16-element coil array and gradient recalled EPI, most brain voxels reach their TSNR limits as predicted by the Kruger and Glover (2001) model. This was not the case using the standard birdcage GE head coil where, neglecting partial volume effects, the only way to improve TSNR and BOLD CNR would be to increase voxel volume. Therefore, in contrast to a standard birdcage coil where increasing spatial

resolution causes a significant reduction in TSNR and BOLD CNR due to relatively low SNR (Merboldt et al., 2000), the 16-channel system increases SNR enough to show enhanced BOLD detection even with a reduction in slice thickness.

Another factor contributing to the improvements in BOLD CNR with thinner slices could be the reduction of intra-voxel tissue heterogeneity. Voxels imaged at standard or low resolution (50–80 mm^3) are more likely to be a mixture of different brain tissue components (GM, WM, CSF, and vasculature) than are higher resolution voxels. Kruger and Glover (2001) have shown that the effects of "physiological noise" are disproportionately distributed among the various tissue compartments such that cortical GM is significantly more sensitive than WM to physiological noise. A likely source for this difference may be differences in neuro-vasculature as the predominant source of physiological noise during fMRI is brain vasculature (Kim et al., 1994). Although decreasing intra-voxel tissue heterogeneity can be accomplished with increased spatial resolution, this solution usually limited by the detrimental influence of physiological noise. Therefore, a sensitive (higher SNR as compared to a standard coil) MRI detector is needed to detect BOLD at increasingly high fMRI spatial resolution. The present data have sufficient SNR to show increased BOLD CNR with 2 mm slices even in regions where there were higher TSNR levels in 4 mm slices. The paradox of

higher TSNR but lower CNR in thicker compared to thinner slices can be interpreted as a significant reduction in noise for thinner slices accomplished by decreasing the partial volume effect (Hyde et al., 2001). Although the source of this noise reduction (i.e. physiological or tissue dependent) was not testable in the current experiment, previous findings of increased physiological noise with field strength and Kruger and Glover's (2001) assertion that tissue heterogeneity noise being-TE sensitive are consistent with this interpretation.

Most fMRI studies assume that the BOLD response is a marker of metabolic demands associated with neuronal processing required for task performance. The current studies show that improved coil/MRI receiver technologies, used at 3 T, will improve the utility of EPI-based fMRI by improving image SNR. The use of the multi-channel digital MRI receiver and 16-element array coil allows for higher resolution EPI images with sufficient SNR to minimize the detrimental effects of noise on BOLD signal detection. The advantages to neuroscience community are several. First, areas susceptible to signal drop are reduced, thus allowing study of areas that previously were not accessible. Second, higher spatial resolution can aid in deciphering intra-regional functional dissociations that are often blurred together using lower resolution (Beauchamp et al., 2004). Third, high resolution scanning decreases intra-voxel tissue heterogeneity, allowing for improved assessment of the contributions made by anatomically distinct tissue types. With the addition of even higher resolution EPI with variable TEs, it should be possible to assess the effects of large veins. Though theoretically plausible, this last point is currently still under investigation. Finally, these improvements can be accomplished using a standard gradient-echo EPI pulse sequence.

Many of the areas showing increased TSNR and particularly increased CNR with 2 mm slices are implicated in memory function in human lesion and animal electrophysiological studies (Squire, 1992; Murray and Wise, 2004; Squire et al., 2004) but have been difficult to image using standard MRI technology. Thus, use of parallel imaging with an arrayed coil could lead to more thorough investigation of the neural substrates of memory function.

Conclusion

Animal electrophysiological and human lesions studies have implicated anterior medial temporal and frontal regions as critically involved such cognitive tasks as declarative memory function, reinforcement evaluation and executive control. Studies of these regions have been limited due to MR imaging artifacts that are particularly prominent in these regions. The relationships among signal-to-noise, slice thickness, and contrast-to-noise were experimentally investigated at 3 T using memory tasks known to activate MTL regions. Significant TSNR improvements with the receive-only multi-element array head coil over the standard quadrature transmit/receive head coil were revealed throughout the imaged region. The greatest TSNR increases are located in brain areas most sensitive to susceptibility artifacts. The results show that thinner slices combined with a 16-element array coil improved TSNR throughout the ventral medial and lateral regions of the MTL. Even greater enhancements were evident when comparisons were made using a measure of BOLD CNR. Thinner slices resulted in greater CNR throughout the anterior temporal lobe and in the ventral orbital frontal gyrus due to the increased SNR available using the 16-channel system. The improvement in TSNR using

thinner slices was associated with decreased intra-voxel MR signal dephasing by suppression of exogenous magnetic field gradients effects at tissue interfaces. Improvements in CNR related to slice thickness reduction may involve interplay among the MR intensity, susceptibility artifacts, physiological noise reduction, and intra-voxel tissue heterogeneity. The advances in the MRI receiver and reception array coil technologies offer new possibilities for robust high field functional studies of MTL.

Acknowledgments

References

Beauchamp, M.S., Argall, B.D., Bodurka, J., Duyn, J.H., Martin, A., 2004. Unraveling multisensory integration: patchy organization within human STS multisensory cortex. Nat. Neurosci. 7, 1190–1192.

Bellgowan, P.S., Binder, J.R., Swanson, S.J., Hammeke, T.A., Springer, J.A., Frost, J.A., Mueller, W.M., Morris, G.L., 1998. Side of seizure focus predicts left medial temporal lobe activation during verbal encoding. Neurology 51, 479–484.

Binder, J.R., Frost, J.A., Hammeke, T.A., Bellgowan, P.S., Rao, S.M., Cox, R.W., 1999. Conceptual processing during the conscious resting state. A functional MRI study. J. Cogn. Neurosci. 11, 80–95.

Bodurka, J., Ledden, P.J., van Gelderen, P., Chu, R., de Zwart, J.A., Morris, D., Duyn, J.H., 2004. Scalable multichannel MRI data acquisition system. Magn. Reson. Med. 51, 165–171.

Brewer, J.B., Zhao, Z., Desmond, J.E., Glover, G.H., Gabrieli, J.D., 1998. Making memories: brain activity that predicts how well visual experience will be remembered. Science 281, 1185–1187.

Buffalo, E.A., Reber, P.J., Squire, L.R., 1998. The human perirhinal cortex and recognition memory. Hippocampus 8, 330–339.

Buffalo, E., Bellgowan, P.S.F., Martin, A., submitted for publication. Distinct roles for medical temporal lobe structures in memory for objects and their locations. J. Neurosci.

Cho, Z.H., Ro, Y.M., 1992. Reduction of susceptibility artifact in gradient-echo imaging. Magn. Reson. Med. 23, 193–200.

Cox, R.W., 1996. AFNI: software for analysis and visualization of functional magnetic resonance neuroimages. Comput. Biomed. Res. 29, 162–173.

Cox, R.W., Hyde, J.S., 1997. Software tools for analysis and visualization of fMRI data. NMR Biomed. 10, 171–178.

Cox, R.W., Jesmanowicz, A., 1999. Real-time 3D image registration for functional MRI. Magn. Reson. Med. 42, 1014–1018.

de Zwart, J.A., Ledden, P.J., van Gelderen, P., Bodurka, J., Chu, R., Duyn, J.H., 2004. Signal-to-noise ratio and parallel imaging performance of a 16-channel receive-only brain coil array at 3.0 Tesla. Magn. Reson. Med. 51, 22–26.

Fischer, F., Ladebeck, R., 1998. Echo-planar imaging image artifacts. In: Schmitt, F., Stehling, M.K., Turner, R. (Eds.), Echo-Planar Imaging, Theory, Technique and Application. Sringer, Germany, pp. 179–200.

Glover, G.H., 1999. 3D z-shim method for reduction of susceptibility effects in BOLD fMRI. Magn. Reson. Med. 42, 290–299.

Glover, G.H., Law, C.S., 2001. Spiral-in/out BOLD fMRI for increased SNR and reduced susceptibility artifacts. Magn. Reson. Med. 46, 515–522.

Golby, A.J., Poldrack, R.A., Illes, J., Chen, D., Desmond, J.E., Gabrieli, J.D., 2002. Memory lateralization in medial temporal lobe epilepsy assessed by functional MRI. Epilepsia 43, 855–863.

Golby, A., Silverberg, G., Race, E., Gabrieli, S., O'Shea, J., Knierim, K.,

Stebbins, G., Gabrieli, J., 2005. Memory encoding in Alzheimer's disease: an fMRI study of explicit and implicit memory. Brain 128, 773–787.

Guo, H., Song, A.W., 2003. Single-shot spiral image acquisition with embedded z-shimming for susceptibility signal recovery. J. Magn. Reson. Imaging 18, 389–395.

Hsu, J.J., Glover, G.H., 2005. Mitigation of susceptibility-induced signal loss in neuroimaging using localized shim coils. Magn. Reson. Med. 53, 243–248.

Hyde, J.S., Biswal, B.B., Jesmanowicz, A., 2001. High-resolution fMRI using multislice partial k-space GR-EPI with cubic voxels. Magn. Reson. Med. 46, 114–125.

Janszky, J., Jokeit, H., Kontopoulou, K., Mertens, M., Ebner, A., Pohlmann-Eden, B., Woermann, F.G., 2005. Functional MRI predicts memory performance after right mesiotemporal epilepsy surgery. Epilepsia 46, 244–250.

Kim, S.G., Hendrich, K., Hu, X., Merkle, H., Ugurbil, K., 1994. Potential pitfalls of functional MRI using conventional gradient-recalled echo techniques. NMR Biomed. 7, 69–74.

Kruger, G., Glover, G.H., 2001. Physiological noise in oxygenation-sensitive magnetic resonance imaging. Magn. Reson. Med. 46, 631–637.

Martin, A., Wiggs, C.L., Weisberg, J., 1997. Modulation of human medial temporal lobe activity by form, meaning, and experience. Hippocampus 7, 587–593.

Menon, R.S., Ogawa, S., Tank, D.W., Ugurbil, K., 1993. Tesla gradient recalled echo characteristics of photic stimulation-induced signal changes in the human primary visual cortex. Magn. Reson. Med. 30, 380–386.

Merboldt, K.D., Finsterbusch, J., Frahm, J., 2000. Reducing inhomogeneity artifacts in functional MRI of human brain activation—Thin sections vs. gradient compensation. J. Magn. Reson. 145, 184–191.

Murray, E.A., Wise, S.P., 2004. What, if anything, is the medial temporal lobe, and how can the amygdala be part of it if there is no such thing? Neurobiol. Learn Mem. 82, 178–198.

O'Kane, G., Insler, R.Z., Wagner, A.D., 2005. Conceptual and perceptual novelty effects in human medial temporal cortex. Hippocampus 15, 326–332.

Schmidt, C.F., Boesiger, P., Ishai, A., 2005a (1 July). Comparison of fMRI activation as measured with gradient- and spin-echo EPI during visual perception. NeuroImage 26 (3), 852–859.

Schmidt, C.F., Degonda, N., Luechinger, R., Henke, K., Boesiger, P., 2005b. Sensitivity-encoded (SENSE) echo planar fMRI at 3T in the medial temporal lobe. NeuroImage 25, 635–641.

Squire, L.R., 1992. Memory and the hippocampus: a synthesis from findings with rats, monkeys, and humans. Psychol. Rev. 99, 195–231.

Squire, L.R., Stark, C.E., Clark, R.E., 2004. The medial temporal lobe. Annu. Rev. Neurosci. 27, 279–306.

Stables, L.A., Kennan, R.P., Gore, J.C., 1998. Asymmetric spin-echo imaging of magnetically inhomogeneous systems: theory, experiment, and numerical studies. Magn. Reson. Med. 40, 432–442.

Stark, C.E., Squire, L.R., 2001. When zero is not zero: the problem of ambiguous baseline conditions in fMRI. Proc. Natl. Acad. Sci. U. S. A. 98, 12760–12766.

Stenger, V.A., Boada, F.E., Noll, D.C., 2002. Multishot 3D slice-select tailored RF pulses for MRI. Magn. Reson. Med. 48, 157–165.

Strange, B.A., Hurlemann, R., Duggins, A., Heinze, H.J., Dolan, R.J., 2005. Dissociating intentional learning from relative novelty responses in the medial temporal lobe. Neuroimage 25, 51–62.

Triantafyllou, C., Hoge, R.D., Krueger, G., Wiggins, C.J., Potthast, A., Wiggins, G.C., Wald, L.L., 2005. Comparison of physiological noise at 1.5 T, 3 T and 7 T and optimization of fMRI acquisition parameters. Neuroimage 26, 243–250.

Wadghiri, Y.Z., Johnson, G., Turnbull, D.H., 2001. Sensitivity and performance time in MRI dephasing artifact reduction methods. Magn. Reson. Med. 45, 470–476.

Wilson, J.L., Jenkinson, M., Jezzard, P., 2003. Protocol to determine the optimal intraoral passive shim for minimisation of susceptibility artifact in human inferior frontal cortex. Neuroimage 19, 1802–1811.

Wong, E.C., Mazaheri, Y., 2004. Shimming of the inferior frontal cortex using an external local shim coil. Proceedings of the International Society of Magnetic Resonance in Medicine (11, Kyoto, Japan, 520).